

# Evaluation of data reduction methods for dynamic PET series based on Monte Carlo techniques and the NCAT phantom

Trias Thireou<sup>a,c</sup>, José Luis Rubio Guivernau<sup>b</sup>, Vassilis Atlamazoglou<sup>d</sup>, Maria Jesús Ledesma<sup>b</sup>, Sotiris Pavlopoulos<sup>a</sup>, Andrés Santos<sup>b</sup>, George Kontaxakis<sup>b,\*</sup>

<sup>a</sup>Biomedical Engineering Laboratory, National Technical University of Athens, Athens, Greece

<sup>b</sup>E.T.S.I. de Telecomunicación, Universidad Politécnica de Madrid, Madrid, Spain

<sup>c</sup>Institute of Computer Science, Foundation for Research and Technology Hellas, Heraklion, Greece

<sup>d</sup>Biophysics Laboratory, Foundation of Biomedical Research of the Academy of Athens, Athens, Greece

Available online 22 September 2006

## Abstract

A realistic dynamic positron-emission tomography (PET) thoracic study was generated, using the 4D NURBS-based (non-uniform rational B-splines) cardiac-torso (NCAT) phantom and a sophisticated model of the PET imaging process, simulating two solitary pulmonary nodules. Three data reduction and blind source separation methods were applied to the simulated data: principal component analysis, independent component analysis and similarity mapping. All methods reduced the initial amount of image data to a smaller, comprehensive and easily managed set of parametric images, where structures were separated based on their different kinetic characteristics and the lesions were readily identified. The results indicate that the above-mentioned methods can provide an accurate tool for the support of both visual inspection and subsequent detailed kinetic analysis of the dynamic series via compartmental or non-compartmental models.

© 2006 Elsevier B.V. All rights reserved.

PACS: 07.05.Pj; 87.58.Mj; 87.58.Fg; 02.70.Vu

Keywords: Dynamic positron-emission tomography; Principal component analysis; Similarity mapping; Independent component analysis

## 1. Introduction

Simulation techniques have become an important and indispensable complement to theoretical derivations, experimental methods and clinical studies in medical imaging research. An important aspect of simulations is the possibility to use realistic computerized phantoms of the human anatomy, to evaluate models of the imaging process and validate image reconstruction and analysis methods. This way the exact anatomy and physiological functions are known, thus providing a gold standard upon which the evaluation and improvement of medical imaging devices and techniques could be based.

The 4D NURBS-based (non-uniform rational B-splines) cardiac-torso (NCAT) phantom [1,2] has been developed

to provide a realistic and flexible model of the human anatomy and physiology. The Geant4 Application for Tomographic Emission (GATE) software package [3,4] is becoming quite popular for positron-emission tomography (PET) simulation and is well validated for a wide range of  $\gamma$ -cameras. Here, we have used these tools to generate a realistic dynamic F-18-fluorodeoxyglucose PET (FDG-PET) thoracic study simulating two solitary pulmonary nodules (SPNs), thus overcoming, among others, ethical and practical problems related to clinical studies.

SPNs are defined as circumscribed parenchymal lung lesions less than 4 cm in size and completely surrounded by normal lung. Although, PET is increasingly being used to detect and characterize SPNs, false negative findings have been reported mainly due to small size, particularly for lesions in the lung bases where respiratory motion may further degrade resolution, and low-grade well-differentiated malignancies such as carcinoids [5,6].

\*Corresponding author. Tel.: +34 91 4533544; fax: +34 91 3367323.

E-mail address: [g.kontaxakis@upm.es](mailto:g.kontaxakis@upm.es) (G. Kontaxakis).

To facilitate the visual analysis of dynamic FDG PET sequences and the calculation of clinically useful parametric information of tracer kinetic models, data reduction and blind source separation (BSS) methods can be applied, which at the same time maintain important information and allow basic feature characterization. Three such methods have been investigated, namely principal component analysis (PCA) [7–9], similarity mapping (SM) [10–12] and independent component analysis (ICA) [13,14].

## 2. Methods

### 2.1. Data generation

GATE has been used for the Monte Carlo simulation (MCS) of the emission and acquisition processes and the open source STIR platform [15] has been used for the reconstruction of the data obtained from the simulations.

The desired time–activity curves (TACs) for each organ have been defined using the NCAT tool (myocardium, blood-pool and two lung lesions of 8 and 12 mm) as shown in Fig. 1. By specifying these curves and other parameters related to the scanner configuration, realistic 3D attenuation and activity distribution maps have been obtained simulating 16 dynamic PET frames at 30 s (frames 1–6), 60 s (frames 7–8), 120 s (frames 9–13) and 300 s (frames 14–16).

These activity maps were used as input to GATE, as voxelized sources, by considering each voxel as a source with an activity level proportional to the voxel's value. The only drawback of using a voxelized source in GATE is the speed of the simulations, as the need for tracking the particles through each individual voxel in the image increases significantly the simulation time. For lessening the computational load only one slice from the NCAT phantom has been simulated with slice thickness of 2.42 mm. The  $\gamma$ -ray emission direction has been restricted to  $\theta$  values in the  $[85^\circ, 95^\circ]$  range and a maximum ring difference of 2 has been set. The scanner geometry of the ECAT EXACT HR+ scanner (Siemens, Knoxville, TN, USA) has been employed.

The FBP algorithm, as implemented in STIR, was used for the image reconstruction, taking into account that the

image quality highly depends on the duration of the each frame. Reconstruction was carried out over a  $261 \times 261$  image grid, with pixel size of 2.25 mm.

### 2.2. Principal component analysis

PCA explains the variance–covariance of a set of variables through a few linear combinations of these (principal components (PC)), in order to achieve data reduction and to facilitate their interpretation. For dynamic PET, these few PCs constitute a reduced set of principal component images (PCI) that can be considered as representing a “summary” of the kinetic information that is contained in original study frames and can therefore be used to extract basic information for an initial evaluation of the dynamic study [7–9]. In order to improve the PCA performance we apply data preprocessing methods [16], namely PCD (data divided column-wise by the column standard deviation) and PCS (data divided column-wise by the column sum) were used during the presented study.

### 2.3. Independent component analysis

ICA is a statistical technique that can be used as a method for BSS. The observed data are assumed to be unknown linear mixtures of unobserved, non-Gaussian and mutually independent source signals (independent components, IC), which can be recovered with no prior information using ICA. The intuitive notion of maximum non-Gaussianity or more classical notions like maximum likelihood estimation–minimization of mutual information can be used to derive objective functions whose optimization enables ICA model estimation [14]. The FastICA algorithm [14] uses approximations of negentropy as a measure of non-Gaussianity, together with a fixed-point iteration scheme, to directly estimate ICs of any non-Gaussian distribution using any nonlinear function  $g(u)$ .

Using the infomax approach [11] spatial (sICA), temporal (tICA) or spatiotemporal (stICA) ICA of 2D images can be estimated. sICA seeks a set of mutually independent source images, tICA seeks a set of independent source time courses, while stICA decomposes an

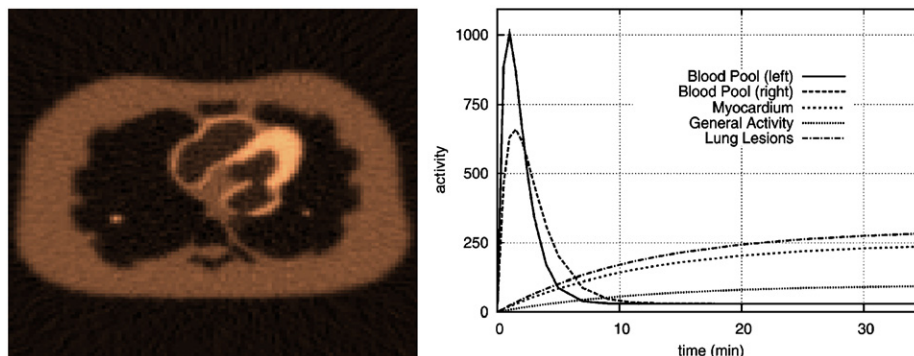


Fig. 1. The last frame of the simulated dynamic PET study and the TACs used for the generation of the data.

image sequence into a set of spatial images and a corresponding set of time courses such that signals in both sets are maximally independent. These approaches are based on the assumption that the probability density function (PDF) of the independent sources is highly kurtotic and symmetric. Since this assumption is not warranted for dynamic PET, we proposed to apply skew-ICA. Skew-ICA embodies the assumption that images are characterized by the skewness (rather than the kurtosis) of their PDF's; an assumption consistent with spatially localized regions of activity [17]. Dynamic PET images are assumed to be the sum of components representing different structures. Each component consists of a time course and a parametric image showing the spatial distribution of the corresponding structure in the target tissue.

#### 2.4. Similarity mapping

SM creates a temporal match of the intensity values of the pixels in the image sequence with those of a selected reference region of interest (rROI) [10,11]. The similarity measures have been applied on dynamic MRI based on the calculation of the correlation (COR) and normalized correlation (NCOR) coefficients [18]. We have recently introduced additional measures more appropriate for low contrast PET: squared sum (SQS) and cubed sum (CS) coefficients [12]. Applying SM to dynamic PET results in one map per slice, where each voxel represents the degree of temporal similarity of the corresponding region to a reference region. Both COR and NCOR measures are normalized for proportional differences, while only NCOR is normalized for additive differences. SQS provides a similarity measure normalized for additive differences and

perfect negatives, whereas CS is normalized for additive differences.

### 3. Results

#### 3.1. Application of PCA

Applying PCA on the synthetic data results in 3 PCIs (Fig. 2). PCI1 resembles the last frame of the dynamic study. In PCI2 the right ventricle, the left atrium and the aorta are depicted with the same color while in PCI3 they are assigned different colors (red vs. blue).

PCD and PCS data transformations do not change the third PCI. However, in PCD\_PCI1 the ventricle and atrium cannot be clearly separated from the myocardium and image noise is slightly higher with respect to PCI1. In PCD\_PCI2 all structures including the lung lesions and the aorta can be readily identified. PCS\_PCI1 resembles PCI2, while in PCS\_PCI2 each structure is assigned a different color according to its kinetic characteristics. Comparing the detectability of SNPs, even the 8 mm lesion is clearly distinguished in the raw and PCD-transformed PCIs, while in PCS-transformed data it is hardly delineated.

#### 3.2. Application of ICA

In the 2nd independent component image (ICI) by skew-stICA, heart structures are better separated than in ICI1 and lesions are visible (Fig. 3). In skew-sICA images are similar to those by skew-stICA. However, increased noise level complicates lesion detection. In skew-tICI1, heart structures are well delineated and lesions are identified easier than in skew-stICI2. Although data transforming prior to skew-ICA does not improve SPNs detection, in

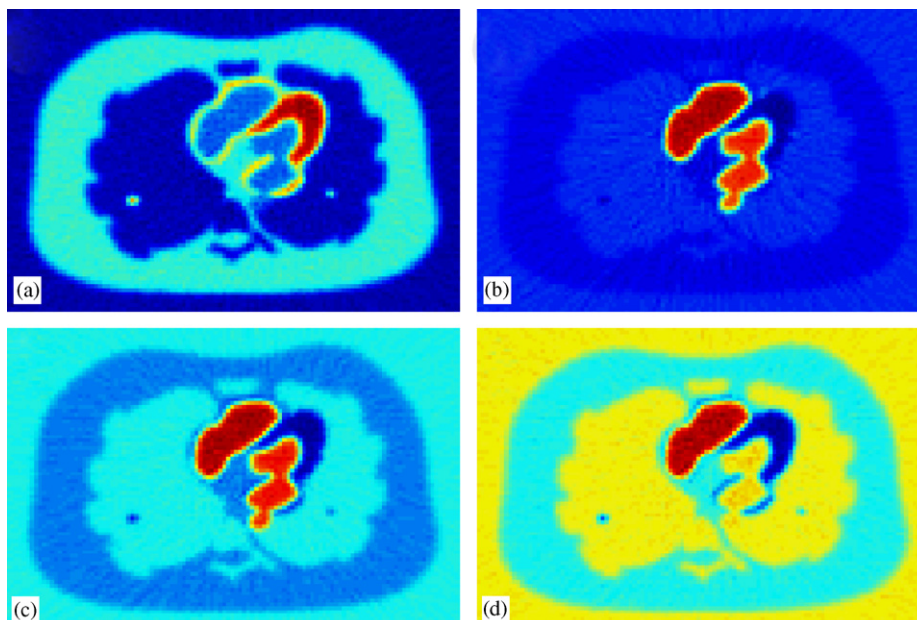


Fig. 2. Principal component images generated using raw data: PCI1 (a), PCI2 (b) and transformed data: PCD\_PCI2 (c), PCS\_PCI2 (d).

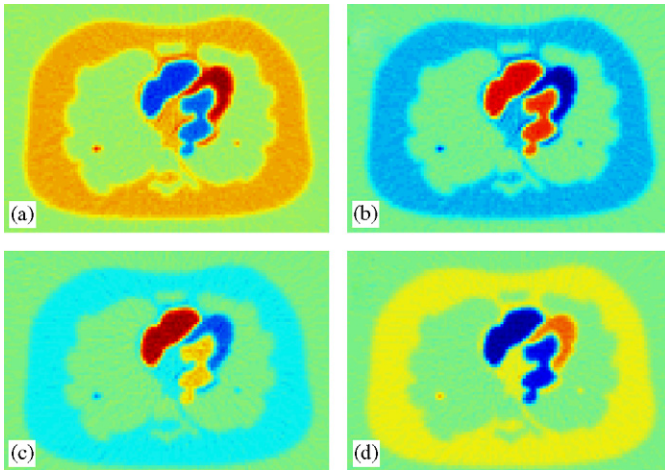


Fig. 3. ICs created using spatiotemporal (a) and temporal (b) skew-ICA on raw data, and temporal skew-ICA on PCD (c) and PCS (d) transformed data.

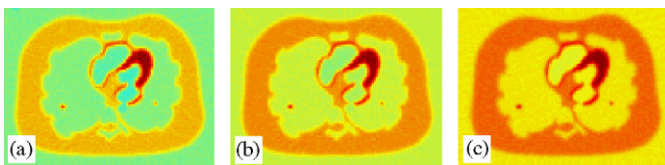


Fig. 4. ICs calculated using Fast-ICA with 'gauss' nonlinearity and raw data (a), PCD-transformed data (b), PCS-transformed data (c).

PCD-preprocessed skew-tICI2 all structures are colored according to their kinetic characteristics, indicating that lesions with different TACs can be better identified.

In the first two ICs the right ventricle, left atrium or both structures are depicted in different color depending on the nonlinearity used to estimate ICs. In ICI3, myocardium, normal tissues and the lung lesions are readily identified and the heart compartments are well delineated, no matter which nonlinearity is used (Fig. 4). PCD preprocessing improves lesion detectability. Applying ICA to PCS-transformed data, results in images with increased noise, but enhanced contrast.

### 3.3. Application of SM

The main goal of this study is to estimate the ability of SM to detect small lesions in the lung. Therefore, reference TACs of the left atrium and normal tissues are used for the calculation of similarity maps (SMaps).

In all cases, SMaps based on COR and NCOR coefficients are very noisy and lesions are rather guessed than clearly identified. Preprocessing the data with the PCD method improves image noise characteristics and lesion detectability (Fig. 5). On the other hand, when using the SQS and CS coefficients to calculate SMaps based on raw data, lesions are readily identified in the resulting parametric images. Moreover in the CS the aorta is also visible. SPNs can be distinguished in SMaps calculated on the transformed data with different levels of contrast and

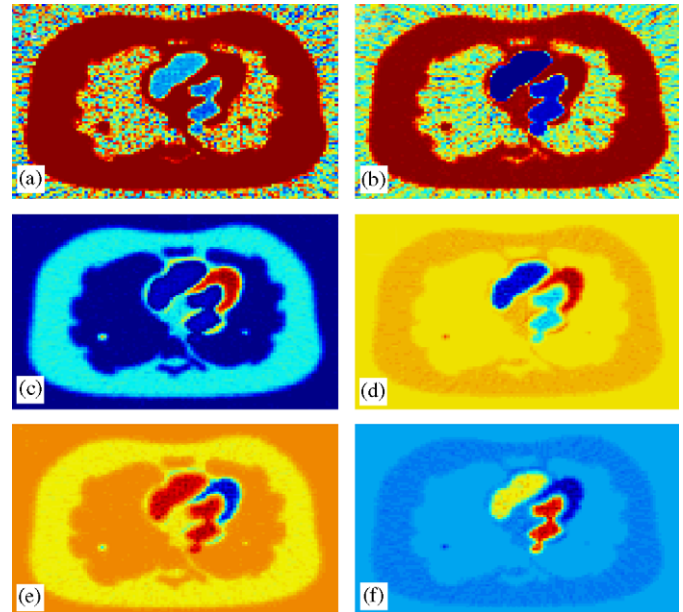


Fig. 5. SM calculated using a reference ROI placed over normal tissue (a–d) and left atrium (e, f) on raw (a, c, d) and PCD-transformed (b, d, f) data. Similarity measures used are NCOR (a, b), SQS (c) and CS (d–f).

clarity. In PCD-preprocessed data, lesions are visible with lower contrast than in the raw-SMaps, whereas in PCS-SMaps, they are hardly detected. However, PCD preprocessing combined with CS enhances the discrimination of structures with different TACs.

## 4. Discussion

Detecting and characterizing SPNs is quite challenging. Imaging techniques that demonstrate the metabolic properties of a lesion have attracted increasing interest, since many lesions remain indeterminate in nature with conventional imaging modalities, such as computed tomography and magnetic resonance imaging. Additionally, histological biopsies are often associated with morbidity and high cost.

FDG-PET is increasingly being used to detect and characterize SPNs. However, accurate detection of small nodules is unlikely, because of scanner resolution and nodule motion during acquisition. Moreover, the specificity of SPNs characterization is rather low in many studies, although several analysis approaches have been used, including qualification by visual comparison of the abnormality with normal structures, semiquantification using standardized uptake ratios (SUR) or lung/background (L/B) ratios or absolute quantification of glycolysis [5,6,19].

We have applied three data reduction and BSS methods: PCA, ICA and SM. These techniques are becoming increasingly popular as a tool for analyzing biomedical data [7–14,20,21]. Based on the presented results, all described methods can generate images where structures with different kinetic characteristics are readily

discriminated and small lung lesions can be detected. Additionally, all techniques are characterized by low computational cost. Therefore, they could be used to support visual inspection of large dynamic PET data sets and facilitate the application of compartmental analysis, since they provide a tool for a more accurate selection of the ROIs on lesions and/or vessels, in order to proceed to further parametric analysis of the dynamic sequences.

Depending on the analysis method and the specific parameters used, data preprocessing prior to applying a data reduction technique may improve or hinder lesion detectability or structure discrimination. Future work in this area will include detailed studies on simulated data with different noise levels and lesion sizes and uptake rates, in order to establish efficient analysis protocols for different cases.

As far as structure identification is concerned, even though PCs and ICs do not coincide with physiologically meaningful TACs and may contain negative values, their shape rather than their absolute values, agrees with the kind of TACs expected, according to the highest intensity regions present in the corresponding images. Therefore, structures with different kinetic characteristics are assigned opposite values and can be easily discriminated.

PCA and ICA calculation are completely automatic, whereas SM requires the placement of a reference ROI and the calculation of the corresponding TAC. All methods require that the image frames for the same tomographic slice are spatially registered.

As a future step, the evaluation of the described methods on studies simulating several benign and malignant lesions and on real clinical cases will be performed. Furthermore,

the application of the analysis techniques on blood volume extraction, blood perfusion and cardiac motion studies will be considered.

### Acknowledgments

This work has been partly supported by the EMIL Network of Excellence (European Commission, contract nr: 503569) and the thematic network IM3 (PI052204) by the Spanish Ministry of Health.

### References

- [1] W.P. Segars, et al., *IEEE Trans. Nucl. Sci.* NS-46 (1999) 503.
- [2] W.P. Segars, et al., *IEEE Trans. Nucl. Sci.* NS-48 (2001) 89.
- [3] D. Strul, et al., *Nucl. Phys. B (Proc. Suppl.)* 125 (2003) 75.
- [4] G. Santin, et al., *IEEE Trans. Nucl. Sci.* NS-50 (2003) 1516.
- [5] I.A. Ho Shon, M.N. Maiey, *Ann. Acad. Med. Singapore* 33 (2004) 166.
- [6] G.U. Hung, et al., *Jpn. J. Clin. Oncol.* 31 (2001) 51.
- [7] F. Pedersen, et al., *Eur. J. Nucl. Med.* 21 (1994) 1285.
- [8] G. Zuendorf, et al., *Hum. Brain Mapping* 18 (2003) 13.
- [9] Z. Chen, et al., *IEEE Trans. Nucl. Sci.* NS-51 (2004) 2612.
- [10] J. Rogowska, et al., *Acta Radiol.* 35 (1994) 371.
- [11] J. Rogowska, et al., *IEEE Trans. Med. Imag.* 14 (1995) 480.
- [12] T. Thireou, et al., *Med. Biol. Eng. Comput.* 43 (2005) 23.
- [13] J.V. Stone, J. Porril, et al., *Neuroimage* 15 (2002) 407.
- [14] A. Hyvarinen, E. Oja, *Neural Networks* 13 (2000) 411.
- [15] STIR project web site <<http://stir.hammersmithimanet.com/>>
- [16] M. Šámal, et al., *Phys. Med. Biol.* 44 (1999) 2821.
- [17] K. Suzuki, T. Kiryu, T. Nakada, *Hum. Brain Mapping* 15 (2002) 54.
- [18] A.O. Boudraa, et al., *Comput. Biol. Med.* 31 (2001) 133.
- [19] K. Shaffer, *Chest* 116 (1999) 519S.
- [20] J.S. Lee, et al., *Nucl. Med.* 42 (2001) 938.
- [21] M. Naganawa, et al., *IEEE Trans. Biomed. Eng.* 52 (2005) 201.